

Effect of Calcination Temperature on Titanium Oxide Nanocrystallites in the Anatase Phase Synthesized By Sol-Gel Route

S. Sharmila Juliet¹, S. Ramalingom², C. Ravidhas³, A. Moses Ezhil Raj^{1*}

¹Department of Physics & Research Centre, Scott Christian College (Autonomous), Nagercoil-629003, India.

²Department of Physics, Vivekananda College, Agasteeswaram-629701, India.

³Department of Physics, Bishop Heber College (Autonomous), Thiruchirapalli-620 017, India.

Corresponding author: A. Moses Ezhil Raj

Abstract: Titanium Oxide (TiO₂) nanocrystalline powders in the anatase phase with tetragonal structure with the point group 4/mmm and space group I4₁/amd–D_{4h}¹⁹ have been synthesized using titanium tetra-isopropoxide as the starting precursor. TG/DTA analysis of the precursor material was carried out in order to fix the calcination temperature for the titanium tetra isopropoxide precursor solution. As-prepared samples were annealed at different temperatures of 400 and 600 °C and their physicochemical properties were examined by means of TG/DTA, XRD, RS, PL, SEM/EDS and DC electrical conductivity studies. X -ray diffraction shows that the as-synthesized samples dried at 100°C in air were amorphous, whereas annealed samples were crystalline and tetragonal structure, belongs to the anatase phase (I4₁/amd). Raman scattering was used to analyze normal Raman active modes of vibration for the confirmation of phase purity of synthesized anatase TiO₂ nanocrystalline with calcination temperatures. Using broad luminescent band, its shape and position were discussed in terms of calcination temperature, particle size and crystallites phase. Morphological observations showed spherical agglomerated grains of micrometer size that constitutes nanosized particles. Elemental analysis indicates that the nanoparticles are essentially TiO₂ without impurities and contaminations. The semiconducting behavior, DC electric conductivity and the activation energy of synthesized samples were also measured by the electrical resistance measurement system.

Keywords: nanocrystalline, sol-gel, luminescent band, conductivity and activation energy

Date of Submission: 27-07-2017

Date of acceptance: 17-08-2017

I. Introduction

Lots of many efforts have been made since the eighties to obtain nanostructured TiO₂ materials with large specific surface area [1]. The energy band structure and photophysical, photochemical and surface properties for nanostructured TiO₂ are quite different from those of its bulk counterparts due to the quantum size effect. TiO₂ has been widely used as a model transition metal oxide because of its simple electronic structure, which is characterized by a filled valence band and an empty conduction band [2]. TiO₂ is an n-type, wide band gap semiconductor and shows excellent optical transmittance in the visible and near infrared regions [3]. It is relatively inexpensive, non-toxic, and biocompatible in nature and exhibits a high photostability in adverse environments. TiO₂ derived materials are important for utilizing solar energy and environmental purification. There are three naturally occurring TiO₂ phases: anatase, rutile, and brookite. It is generally accepted that the TiO₂ in anatase phase is the most active phase because of its metastable phase and is widely used as a photocatalyst [4]. Applications of nanosized anatase TiO₂ are primarily determined by its physicochemical properties such as crystalline structure, particle size, surface area, porosity and thermal stability. Anatase TiO₂ has attracted much attention as a key materials for dye- sensitized solar cells [5], gas sensors [6], electrochromic devices [7], pigments [8], catalyst [9], light- sensitizers [10], electro chromophores[11], optoelectronics and ceramic membrane [12]. New physical and chemical properties emerge when the size of material becomes smaller and smaller, and down to the nanometer scale. Among the unique properties of nanomaterials, the movement of electrons and holes in semiconductor materials is primarily governed by the well-known quantum confinement and the transport properties related to phonons and photons are largely affected by the size and geometry of the materials [13-16]. The specific surface area and surface to volume ratio increases dramatically as the size of material decreases [17]. The high surface area brought about by the small particle size in beneficial to many TiO₂ based devices, as it facilitates reaction or interaction between the devices and the interacting media, which mainly occurs on the surface or at the interface and strongly depends on the surface area of the material. Thus, the performance of nano TiO₂ based devices is largely influenced by the particle size of the TiO₂ building units, apparently about the size of nanometer range.

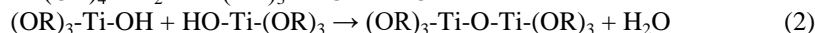
A variety of chemical syntheses have been developed so far for the synthesis of TiO₂ nanoparticle for several years and sol-gel synthesis has proven to be effective for the synthesis of TiO₂ in the form of powders with controlled nanostructure and surface properties [18]. The sol-gel process is called “soft chemistry” because reactions occur at low temperature and low pressure. The obtained as-prepared TiO₂ nanoparticles were actually not crystalline in the anatase phase, but may be in an amorphous structure. The as-synthesized nanoparticles will offer another possibility to design various TiO₂ related phases by post heat treatment methods. Since the crystalline phase and size are in turn sensitive to calcination temperature, a step has been devoted to studying its calcination effect on structure, phase, morphological, optical and electrical properties.

Keeping the above aspects in view, we report in this paper the synthesis of ultra-fine nanostructured TiO₂ photocatalyst in anatase phase through cost effective sol-gel technique using titanium tetra-isopropoxide as a starting precursor material and the effect of calcination temperature on the structural, optical and electrical properties were analyzed with the variations of calcination temperatures.

II. Experimental Procedure

2.1. Powder Synthesis

Titanium oxide nanocrystalline powders in the anatase phase have been prepared by using 8 ml of titanium tetra-isopropoxide [Ti(OiPr)₄] as the starting precursor and was then dissolved in 50 ml ethanol as solvent under constant magnetic stirring [19]. The sol obtained after 45 min was then converted into a gel by adding it to 100 ml of deionized water. The gel obtained was left at room temperature. After some time the white powder settled down was then washed with distilled water and ethanol followed by centrifugation for three times to remove impurities. Finally, the powders were dried in air at 100 °C for 1hr, and then calcined at 400 and 600 °C for 2hrs in a muffle furnace with a heating rate of 10 °C per min then weighed for the yield of the process. The titanium precursor undergoes two main reactions: hydrolysis and condensation during synthesis (Eqs. 1 and 2) [20].



2.2. Powder Characterization

The thermogravimetric analysis of the synthesized samples was taken using PERKIN-ELMER DIAMOND TG/DTA apparatus ranging from 25 °C to 1000 °C at a heating rate of 10 °C/min under nitrogen atmosphere. Structural investigations were performed using X-ray diffraction spectra recorded in the PHILIPS X'PERT-PRO diffractometer with the continuous scanning of the sample was done in the θ -2 θ mode using a CuK_α target of wavelength $\lambda=1.5406 \text{ \AA}$ of setting step size of 0.03°. Raman spectra of the synthesized nano TiO₂ powder samples were recorded at room temperature using RFS 27 FT-RAMAN BRUKER spectrometer. Photoluminescence spectrum was carried out by JOBIN YVON FLURO LOG-3-11 Spectro-fluorimeter using Xenon lamp - 450W as a source within the range 180-1550 nm. Both excitation radiation and emitted radiation can be scanned. Morphologies of particles were observed via scanning electron microscopy (SEM) JEOL Model JSM – 6390 LV and compositions of the synthesized particles were determined by energy dispersive spectrum (EDS) using a JEOL Model JED -2300 microscope. The DC electric conductivity was also measured by the varying the temperature from room temperature to 150 °C using high-temperature two-probe setup.

III. Results And Discussion

3.1. Thermal Gravimetric Analysis

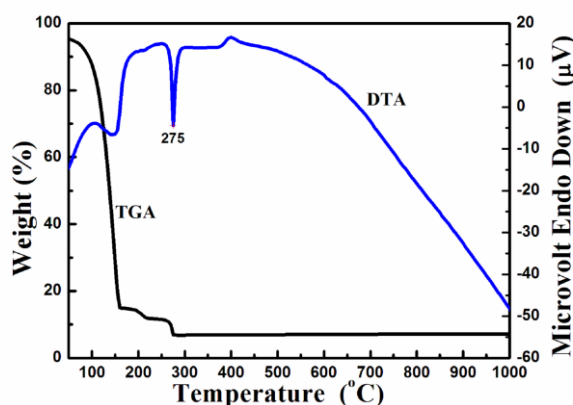


Figure.1: TGA/DTA traces of titanium tetra iso-propoxide precursor solution.

Figure.1 shows the typical thermal analysis of the titanium tetra iso-propoxide (TTIP) precursor used in the synthesis of anatase TiO₂ nanoparticles. The required calcination temperature for the formation of TiO₂ phase was ridged from thermal decomposition pattern of TTIP. As observed the thermal degradation has occurred in three steps. The first degradation starts from room temperature to 160 °C, which is due to the removal of the co-ordinated water from the starting precursor to a mass loss of about 85 %. The second degradation occurs in the temperature ranges 191 to 215 °C that corresponds to 3 % mass loss due to the elimination of physisorbed water and removal of organic residues [21]. The third stage of weight loss is observed at about 250 °C could be attributed to partial dehydroxylation of Ti(OH)₄, which leads to transformation of amorphous phase to a crystalline structure of TiO₂. Above 275 °C, the product remains stable without mass loss, indicating the thermal stability of the crystalline TiO₂ sample. Hence TGA thermal analysis confirms the required temperature for the formation of TiO₂ from the starting precursor.

Similar to TGA, DTA curve shows desorption of water that occurs at a low temperature between 100 and 146 °C and achieves maximum nearly as 146 °C. The observed endothermic peak for this decomposition is due to the physically adsorbed water in the studied samples [22]. The second and third decomposition stages observed in TGA give rise to well-defined endothermic peaks in DTA curve. The endothermic peak at about 150 °C indicates the beginning of the decomposition of the residual organic precursor, titanium tetra isopropoxide. The third peak at 275 °C is a broad maximum with a plateau that could be related to the complete decomposition of the organic residues along with the removal of OH groups(dehydroxylation)leading to the TiO₂ formation. This phase transformation was also confirmed through Raman and XRD studies and this range anatase was found in accordance with the literature [23]. The exothermic peak at about 400 °C exhibited obvious decalescence phenomena, possibly resulting from amorphous to crystalline anatase phase. Since decomposition is complete after 400 °C, the calcination temperatures fixed are not exceeding 600 °C. At these temperatures, TiO₂ nanoparticle in its anatase phase is obtained without any trace of impurities. On further increasing the temperature, gradual changes in the DTA curve denotes conversion of anatase to rutile. TGA analysis thus confirms the required temperature range for the formation of TiO₂ from the starting precursor.

3.2. XRD Analysis

3.2.1. Structural studies

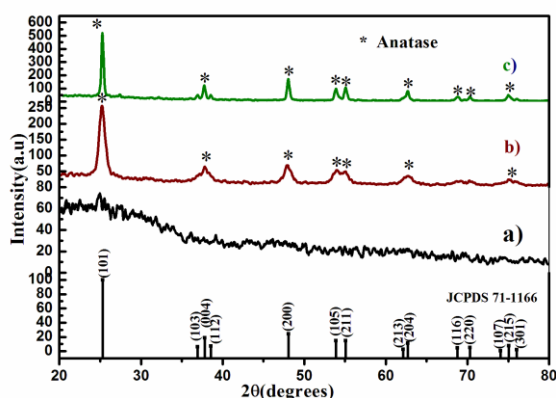


Figure.2: XRD patterns of Sol –gel synthesized anatase TiO₂ nanopowder a) as prepared b) calcined at 400 °C and c) calcined at 600 °C for 2h with the JCPDS standard.

The XRD patterns of the as-synthesized TiO₂ nanopowder dried at air showed an amorphous which revealed a broad pattern of low intensity, which is shown in Figure. 2 imply small crystallite size [24]. The as-synthesized TiO₂ nanoparticles then calcined at different temperatures, such as 400 °C and 600 °C. The as-synthesized amorphous phase could transform into anatase phase at 400 °C, which means the amorphous TiO₂ had been crystallized to anatase after calcination at 400 °C for 2h. For increasing calcination temperature from 400 °C to 600 °C, the peak intensities of anatase increased, indicating the improvement of crystallization of anatase phase. As the calcination temperature increases the anatase peaks becoming higher and thinner that shows the increase in crystallite size.

All the synthesized TiO₂ powder samples have anatase phase with tetragonal structure. The presence of crystalline TiO₂ in the anatase phase was compared with standard JCPDS file no 71- 1166. Diffraction peaks at 2θ = 25.25° and 48° strongly confirm the formation of TiO₂ in the anatase phase without shoulders indicating zero influence of other phases like rutile and brookite. It is well known that the anatase phase is thermodynamically stable for smaller crystallites.

3.2.2. Crystalline size

The average crystallite sizes of calcined crystalline powders at 400 and 600 °C were evaluated by the Scherrer's diffraction formula [25], $D = K\lambda/\beta\cos\theta$. Where, λ is 0.15406 nm corresponding to irradiation wavelength, K is a shape factor that varies with the method of taking the breadth lies between 0.89 and 1.39, here in this work $K=0.94$ for calculation purpose, β is the full width at half maximum of strongest line and θ is the Bragg angle of the most intense peak at a specific phase. The crystalline size is measured for the sample of TiO_2 400 using Scherrer's equation was 14.66 nm, demonstrating that each grain corresponds in average to a single crystallite. The crystallite size of the anatase phase increased from 14.66 nm to 41 nm on increasing the calcination temperatures to 600 °C. The crystallite size for the anatase samples also found by Scherrer's plot and the obtained values are listed in Table 1. Thus the calcination temperature profoundly influenced the crystallite size of the synthesized TiO_2 particles.

3.2.3. Lattice parameter

The lattice parameters of the catalysts were measured using interplanar spacing that relates to Miller indices for the tetragonal system $1/d^2 = (h^2+k^2)/a^2 + l^2/c^2$, a and c are the lattice parameters (for tetragonal $a=b \neq c$). The calculated lattice parameters and crystallite sizes for all calcined samples were listed in Table 1. Obtained values are almost equal to the JCPDS standards. The volume of the unit cell for the samples was determined by using the relation, $V = a^2c$. Where 'a' and 'c' are the lattice parameters. And the densities were calculated using the formula, $\rho = (FW \times z \times 1.66)/V$. Where, FW is the formula weight, ($FW = 79.90$ gm/mol), z is the number of unit cells (for anatase $z = 4$) and V is the unit cell volume. The calculated unit cell volume and crystalline densities for all calcined samples were listed in Table 1. Obtained values are almost equal to the JCPDS standards (No: 77-1166).

Table 1: Structural and electrical parameters of the synthesized anatase TiO_2 nanoparticle

Sample Details	² Crystallite Size (nm)			³ Grain size SEM (nm)	Lattice parameters		Microstrain $\epsilon \times 10^{-4}$	Unit cell volume $V (\text{\AA}^3)$	Density ρ (g/cm ³)	Electrical Data	
	Scherrer Formula	Scherrer Plot	W-H plot		a (Å)	c (Å)				σ mho/m	E_a (eV)
TiO_2	-	-	-	365	-	-	-	-	-	1.32	0.774
TiO_2 400	14.66	16.86	9.81	437	3.788	9.499	-15.9	136.34	3.891	2.58	0.638
TiO_2 600	41.00	42.22	33.2	493	3.787	9.518	-4.32	136.49	3.887	7.16	0.623
¹ JCPDS					3.784	9.515		136.25	3.895		

1- Standard lattice parameters from JCPDS 71-1166. 2- Crystallite size from XRD analysis. 3- Mean grain size from SEM analysis. σ - DC Conductivity. E_a - Activation Energy.

3.2.4. Microstrain

The traditional line profile analysis method like Williamson-Hall plot [26] is useful for a preliminary screening of the data. Williamson-Hall plots for TiO_2 nanopowder samples calcined at various temperatures were drawn. From the W-H plot, mean crystalline size of calcined TiO_2 powder and the amount of internal strain created within the samples were determined by this method according to the equation: [27] $\beta_D = K\lambda/D\cos\theta + 4\epsilon\tan\theta$. Where, β is the full-width of the peak at half of its maximum intensity, θ is the Bragg angle, λ is the wavelength of the X-ray used, D is the average crystallite size, ϵ is the internal microstrain in the powder and K is a shape factor that varies with the method of taking the breadth ($0.89 < K < 1.39$), here in this work $K=0.94$. The crystalline size and the mean strain of the samples were presented in Table 1. It shows that the microstrain decreases when calcination temperature increases because of the increase in crystallite size.

3.3. FT-Raman analysis

Raman spectroscopy provides additional information about the anatase crystallinity. Typical Raman spectroscopy is a powerful tool in the study of TiO_2 for its high sensitivity to the microstructure. Raman Spectra of the TiO_2 nanopowders calcined at different temperatures are shown in Figure.3.

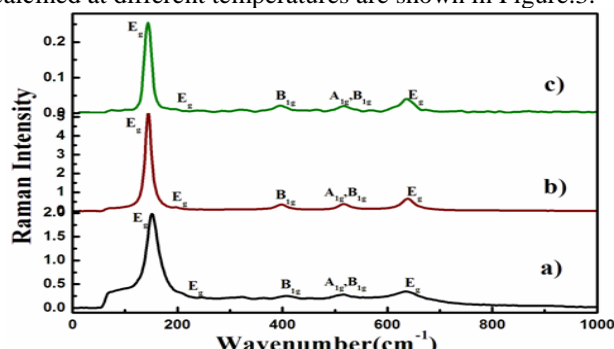


Figure.3: FT-Raman spectra of synthesized anatase TiO_2 nanoparticles a) as- prepared b) calcined at 400 °C and c) calcined at 600 °C for 2hrs.

According to Factor group theory, Anatase TiO_2 has ten vibrational modes: $A_{1g}+1A_{2u}+2B_{1g}+1B_{2u}+3E_g+2E_u$. Among them A_{1g} , B_{1g} , and E_g are Raman active, the A_{2u} and E_u are infrared active and the B_{2u} is inactive both in Raman and Infrared spectra [28]. From Figure, it is obvious that the observed bands at 144 cm^{-1} (E_g), 196 cm^{-1} (E_g), 397 cm^{-1} (B_{1g}), 516 cm^{-1} (A_{1g} & B_{1g}) and 639 cm^{-1} (E_g) corresponds to the Raman active modes ($A_{1g}+2B_{1g}+3E_g$) that belong to the space group D_{4h} ($I41/amd$). For Rutile phase, there are 18 normal modes with space group $d4h$ ($P42/mnm$): $A_{1g}+A_{2g}+B_{1g}+B_{2g}+E_g+2A_{2u}+2B_{1u}+4E_u$. Where, A_{1g} , B_{1g} , B_{2g} and E_g vibrational modes are Raman active, the A_{2u} and E_u vibrational modes are infrared active [29]. The absence of these Raman bands corresponding to rutile phase of titanium oxide, confirms the phase purity of the synthesized anatase TiO_2 nanoparticle [30]. On increasing the calcination temperature to $600\text{ }^\circ\text{C}$, the most intense E_g peak is red-shifted and its FWHM decreases. The shift of observed modes is in accordance to the literature data [31]. This is the well-known behavior of increase in nanoparticle size with calcination temperature and is explained by phonon confinement.

3.4. Photoluminescence

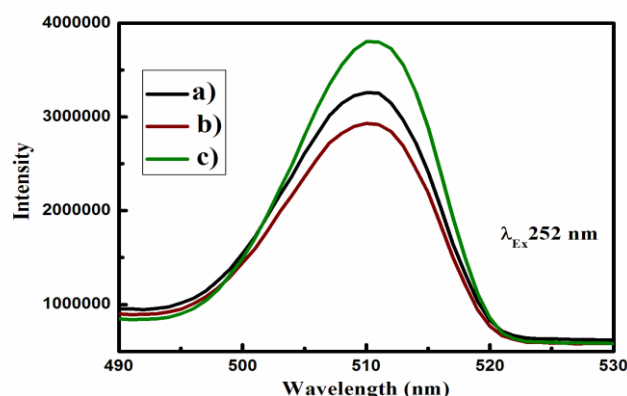


Figure.4: PL spectra of synthesized anatase TiO_2 nanoparticles a) as- prepared b) calcined at $400\text{ }^\circ\text{C}$ and c) calcined at $600\text{ }^\circ\text{C}$ for 2h.

Fluorescence emission spectrum of the synthesized anatase Titanium Oxide samples is shown in Figure.4. The emission peak is found at 510 nm with respect to the excitation peak at 252 nm . Under the laser irradiation of 252 nm , the anatase nanocrystals displayed strong visible light emission at about 510 nm , which is assigned to the oxygen vacancy with one trapped electron, F^+ center [32]. The line shape and position of this broad luminescence band vary with particle size and a crystalline phase. Intensity variations suggest that the photoluminescence (PL) spectrum of nanopowder with larger crystallite size is dominated by a radiative recombination of electrons via intrinsic surface states [33]. As the process temperature is less for the formation of anatase phase with smaller particles, a blue shift is visible in the emission peaks due to the available surface energy that induces quantum confinement. This is due to the presence of more oxygen vacancies on the surface of titanium oxide nanoparticles and the size of the particle was fine and hence the average distance of the electrons could make the oxygen vacancies very easily bind electrons to form is excitons. Thus, the exciton energy level near the bottom of the conduction band could make the strong excitonic spectrum [34, 35]. This narrower band gap will facilitate easy excitation of electrons from the valance band to the conduction band which will result in higher photocatalytic activities [36].

3.5. Surface Analysis

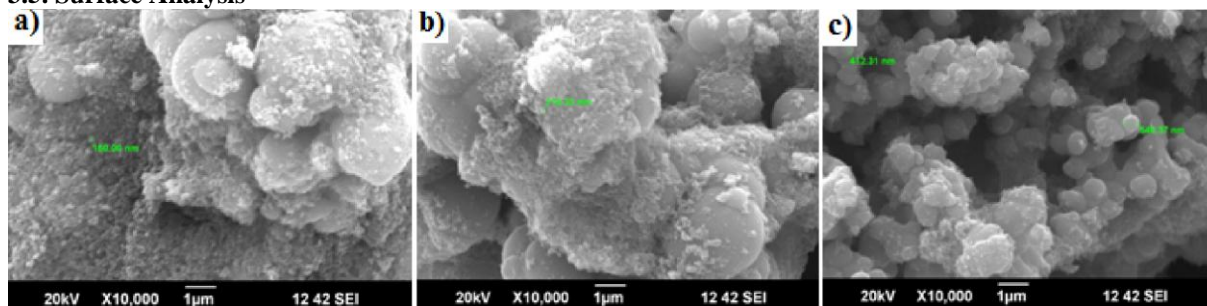


Figure.5: SEM images of the synthesized anatase TiO_2 nanoparticles a) as- prepared b) calcined at $400\text{ }^\circ\text{C}$ and c) calcined at $600\text{ }^\circ\text{C}$ for 2hrs.

The microstructure of the synthesized nanopowders was observed and morphology was analyzed using Scanning Electron Microscopy. SEM micrograph of synthesized TiO₂ nanopowder sample with different annealing temperatures is shown in Figure.5. As for as-synthesized powder, it is obvious that fine particles agglomerate to form larger secondary particles. The almost similar microstructure was observed for the powders calcined at 400 °C. However, interconnected spherical particles with a smooth surface were observed for the powder calcined at 600 °C. Thus the SEM micrographs indicate that the particle size is nearly uniform and spherical throughout the surface in the sample, there is no change in morphology when the annealing temperature increases from 400 °C to 600 °C. Observed spherical particle formation for all the samples has been observed and the mean diameter is tabulated in Table 1.

3.6. Elemental Analysis

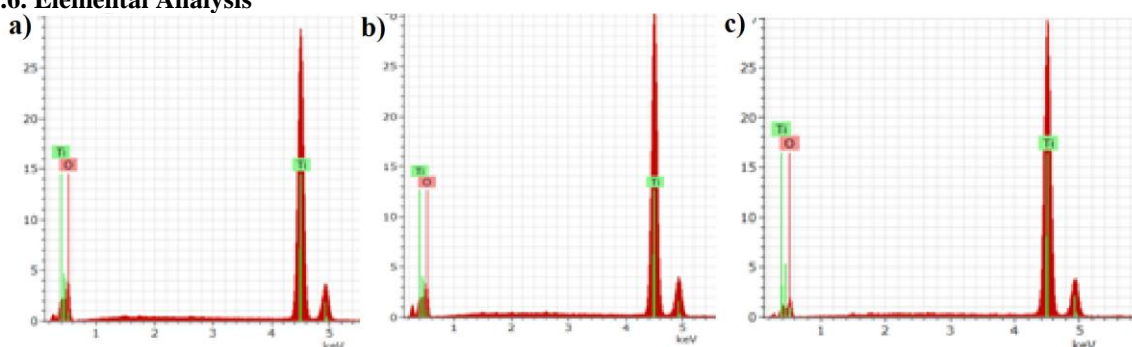


Figure.6: Energy dispersive spectrum of TiO₂ nanoparticles a) as- prepared b) calcined at 400 °C and c) calcined at 600 °C for 2hrs.

The EDS result of the synthesized TiO₂ nanopowder samples in anatase phase is shown in the Figure. 6. It reveals that all powder samples do not include any chloride anion which indicates that these ions are washed out completely at the washing stage. No impurity elements could be detected within the detection limits shows the purity of the prepared samples. The hardly visible maximum located at 0.5 keV is connected with the oxygen characteristic line. However, the presence of Ti⁴⁺ in the prepared anatase TiO₂ nanocrystallite can be viewed from the peak positioned at 4.5 keV. The 76 % of titanium and 24 % of oxygen spots in the examined powder samples TiO₂, TiO₂ 400 and TiO₂ 600 confirm the presence of Titanium Oxide.

3.7. DC Conductivity

For electrical measurements the powders were uniaxially pressed into pellets of 13 mm in diameter, 2 mm in thickness using Hydraulic pellet press of type KP with the load of 5tons and sintered at 200 °C for 1hr with a heating rate of 10 °C per min. In order to study the mechanisms of conductivity, it is convenient to plot ln (σ) as a function of 1000/T. Figure.7 shows the relation between of ln σ versus 1000/ T for TiO₂ with different calcination temperatures in the temperature range of room temperature 30 °C to 150 °C. The plots are further analyzed to calculate the activation energies E_a from the slopes of the straight lines in all the synthesized samples using equation [37]: $\sigma = \sigma_0 e^{(-E_a/k_B T)}$, where, σ₀ – pre-exponential factor or temperature independent conductivity, E_a - activation energy, k_B -Boltzmann constant, and T- temperatures.

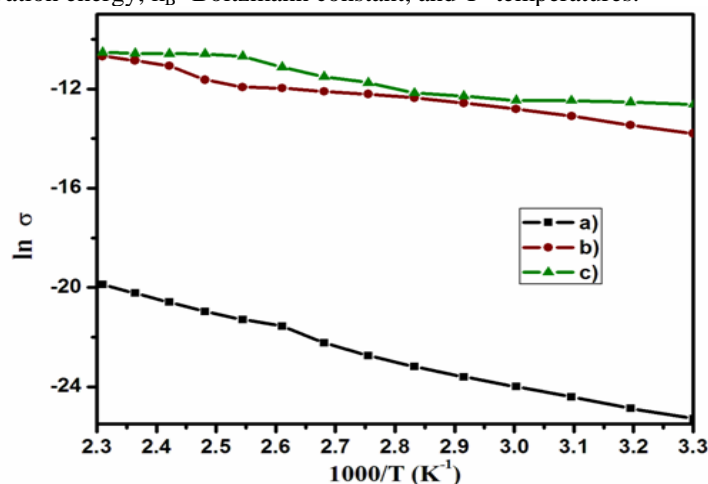


Figure.7: Arrhenius plots of the conductance in dry air for the synthesized anatase TiO₂ nanopowder samples a) as- prepared b) calcined at 400 °C and c) calcined at 600 °C for 2 hrs.

It is clear that from the Figure.7, in all the samples, the plots are nearly straight lines, indicating that the conduction in these samples through an activated process having single activation energy in the given temperature range reveals that the conductivity increases with increase in temperature, such as the general characteristics of the semiconductor with increasing temperature lead to an increase in the number of electron-hole pairs result in an increased conductivity. The activation energy of the samples can be determined from the slopes of the straight lines. The analysis of the conductivity data yields the activation energies of the donor levels, which are given by an Arrhenius plot. The conduction mechanism of the activation energy (E_a) at the given lower temperatures range is due to carrier excitation into localized state at the edge of the band. All the samples would show a perfect semiconducting behavior and hence increase in conductivity with increasing temperature as expected. An increase in conductance of as-synthesized TiO_2 may be ascribed to the presence of adsorbed water molecules on the surface of pure titanium oxide before calcination temperature.

The electrical and physical properties of semiconductor metal oxides are mostly affected by the depth of the space charge region within the crystallite or grain. If the size of the particle is smaller, the electrical properties of the material are strongly affected by the surface phenomena. H. Tang et.al [38] reported that the nanocrystalline TiO_2 metal oxides with the crystallite size of 20 nm represent such material, where the depletion can develop very well through the entire grain and affect its conductivity. Such homogeneous charge concentration in the crystallite or grain leads to the case of flat band potential. Development of the space charge region in nanocrystalline materials is strongly related to the thermal conditions, thus along with the temperature increase the concentration of electron increases and as a result, the width of the depletion layer decreases. In the case of large grains additionally, transport from one crystallite or grain to another as well considered [39].

The calculated activation energy of the synthesized TiO_2 samples with different calcination temperatures was tabulated in Table.1 as 0.774, 0.638, 0.623 eV, which decreases with increase in calcination temperature as the decrease in the lattice strain and the increase in crystallite size of initial anatase phase induced the decrease in the activation energy. However, the faster decrease of the lattice strain in the as-prepared sample during the lower gelatinisation time with the increase of the calcination temperature from 400 °C to the transition onset point gave rise to the larger activation energy. As a result, the size of the crystallites and the activation energy depended on the value of the lattice strain and its circumstances. Thus the conductivity of prepared samples increases with the temperature significantly due to semiconducting behavior and also it is increasing due to the grain size effect while activation energy increases with a decrease in grain size.

IV. Conclusions

TiO_2 nanoparticles have been synthesized in its anatase phase, by varying the calcination temperature. Studies have been carried out to find the effects of calcination temperature on structure, phase, morphology, optical and electrical properties. On increasing the calcination temperature, TiO_2 transforms from amorphous to anatase at 400 °C and 600 °C, accompanied by an increase in crystal grain size. The results obtained from XRD, RS and PL investigations facilitate assigning the obtained product to anatase structure. SEM measurements were used to examine the spherical morphology of samples and the phase purity of the synthesized anatase samples was also confirmed by EDS analysis. The DC conductivity measurements revealed the semiconducting nature of the synthesized samples and the activation energy values were extracted from Arrhenius plot, which decreases with increase in calcination temperature.

References

- [1] O. Masson, V. Rieux, R. Guinebretière and A. Dager, (1996) "Size and shape characterization of TiO_2 aerogel nanocrystals", *Nanostruct. Mater.* **7** 725-731.
- [2] R. Asahi, Y. Taga, W. Mannstadt, and A. J. Freeman, (2000) "Electronic and optical properties of anatase TiO_2 ," *Phys. Rev. B.* **61** 7459-7465.
- [3] U. Diebold, (2003) "The surface science of titanium dioxide," *Surf. Sci. Rep.*, **48** 53-229.
- [4] S. Sakka, (2006) "Current sol-gel activities in Japan," *J. Sol-Gel Sci. Technol.*, **37** 135 -140.
- [5] J. N. Hart, D. Menzies, Y. B. Cheng, G. P. Simon and L. Spiccia, (2006) "Microwave processing of TiO_2 blocking layers for dye-sensitized solar cells," *J. Sol-Gel Sci. Technol.*, **40** 45-54.
- [6] D. Kim, A. Rothschild, D. J. Yang and H. L. Tuller, (2008) "Macroporous TiO_2 thin film gas sensors obtained using colloidal templates," *Sens. Actuators B. Chem.*, **130** 9-13.
- [7] M. G. Kang, K. S. Ryu, S. H. Chang, N. G. Park, J. S. Hong, et al (2004). "Dependence of TiO_2 film thickness on photocurrent-voltage characteristics of dye-sensitized solar cells," *Korean Chem. Soc.*, **25** 742-744.
- [8] G. Pfaff and P. Reynders, (1999) "Angle-Dependent Optical Effects Deriving from Submicron Structures of Films and Pigments," *Chem. Rev.*, **99** 1963-1982.
- [9] P. S. Awati, S. V. Awate, P. P. Shah and V. Ramaswamy, (2003) "Photocatalytic Decomposition of Methylene Blue Using Nanocrystalline Anatase Titania Prepared by Ultrasonic Technique," *Catal. Commun.*, **4** 393-400.
- [10] M. Gratzel, "Photoelectrochemical cells", (2001) *Nature.*, **414** 338-344.
- [11] I. C. Cheon, M. S. Lee, H. K. Shim, and Y. I. Kim, (2003) "Effect of Phosphonate-Functionalized Surface Modification on Nanocrystalline TiO_2 Film Electrode," *Bull. Korean Chem. Soc.*, **24** 1535-1537.
- [12] M. Sreemany and S. Sen, (2004) "A simple Spectrophotometric method for determination of the Optical constants and Band gap energy of multiple layer TiO_2 Thin films," *Mater. Chem. Phys.*, **83** 169-177.
- [13] A. P. Alivisatos, (1996) "Perspectives on the Physical Chemistry of Semiconductor Nanocrystals," *J. Phys. Chem.*, **100** 13226-

- 13239.
- [14] A. P. Alivisatos, (1996) "Semiconductor Clusters, Nanocrystals, and Quantum Dots," *Science*, **271** 933-937.
- [15] C. Burda, X. Chen, R. Narayanan and M. A. El-Sayed, (2005) "Chemistry and Properties of Nanocrystals of Different Shapes," *Chem. Rev.*, **105** 1025-1102.
- [16] C. B. Murray, C. R. Kagan, and M. G. Bawendi, (2000) "Synthesis and Characterization of Monodisperse Nanocrystals and Close-Packed nanocrystal Assemblies," *Annu. Rev. Mater. Sci.*, **30** 545-610.
- [17] X. Chen, Y. Lou, S. Dayal, X. Qiu, R. Krolicki, C. Burda, C. Zhao, and J. Becker, (2005) "Doped semiconductor nanomaterials," *J. Nanosci. Nanotechnol.*, **5** 1408-1420.
- [18] O. Carp, C. L. Huisman, and A. Reller, (2004) "Photoinduced reactivity of titanium dioxide", *Progr. Solid State Chem.*, **32** 33-177.
- [19] A. Golubovic, M. Scepanovic, A. Kremenovic, S. Askrabic, V. Berec, Z. Dohcevic-Mitrovic, Z. V. Popovic, (2009) "Raman study of the variation in anatase structure of TiO₂ nanopowders due to the changes of sol-gel synthesis control", *J. Sol-Gel Sci. Technol.*, **49** 311-319.
- [20] G. W. Brinker, and C. Jeffrey, Scherer, "Sol-gel science: the physics and chemistry of sol-gel processing", Academic press, INC, New York (2013).
- [21] M. S. Lee, G. D. Lee, S. S. Park and S. S. Hong, (2003) "Synthesis of TiO₂ nanoparticles in reverse microemulsion and their photocatalytic activity," *J. Ind. Eng. Chem.*, **9** 89-95.
- [22] P. Jeevanandam, Yu. Koltypin, A. Gedanken, (2002) "Preparation of nanosized nickel aluminate spinel by a sonochemical method", *Mater. Sci. Eng. B.*, **90** 125-132.
- [23] Z. B. Zhang, C. C. Wang, R. Zakaria and J. Y. Ying, (1998) "Role of Particle size in Nanocrystalline TiO₂-based Photocatalysts," *J. Phys. Chem B.*, **102** 10871-10878.
- [24] G. Sarala Devi, and Takeo Hyodo, Yasuhiro Shimizu and Makoto Egashira, (2002) "Synthesis of mesoporous TiO₂-based powders and their gas-sensing properties," *Sens. Actuators, B Chem.*, **87** 122-129.
- [25] J. I. Langford and A. J. C. Wilson, (1978) "Scherrer after Sixty Years: A Survey and. Some New Results in the Determination of Crystallite Size," *J. Appl. Crystallogr.*, **11** 102-113.
- [26] G. K. Williamson and W. H. Hall, (1953) "X-ray line broadening from filed aluminium and wolfram," *Acta Metall. Mater.*, **1** 22-31.
- [27] P. Scardi, M. Leoni, and R. Delhez, (2004) "Line broadening analysis using integral breadth methods: A critical review," *J. Appl. Crystallogr.*, **37** 381-390.
- [28] T. Ohsaka, (1980) "Temperature dependence of the Raman spectrum in anatase TiO₂," *J. Phys. Soc. Japan.*, **48** 1661-1668.
- [29] S. S. Chan, I. E. Wachs, L. L. Murrell, L. Wang and W.K. Hall, (1984) "In situ laser Raman spectroscopy of supported metal oxides," *J. Phys. Chem.*, **88** 5831-5835.
- [30] H. L. Ma, J. Y. Yang, Y. Dai, Y. B. Zhang, B. Lu et al., (2007) "Raman study of phase transformation of TiO₂ rutile single crystal irradiated by infrared fem to second laser," *Appl. Surf. Sci.*, **253** 7497-7500.
- [31] K. Gao, (2007) "Strongly intrinsic anharmonicity in the low-frequency Raman mode in nanocrystalline anatase TiO₂", *Physica. B.*, **398** 33-37.
- [32] N. Ghows and M. H. Entezari, (2010) "Ultrasound with low intensity assisted the synthesis of nanocrystalline TiO₂ without calcination," *Ultrason. Sonochem.*, **17** 878-883.
- [33] Y. Lei, L. D. Zhang, G. W. Meng, G. H. Li, X. Y. Zhang, C. H. Liang, W. Chen, S. X. Wang, (2001) "Preparation and photoluminescence of highly ordered TiO₂ nanowire arrays", *Appl. Phys. Lett.*, **78** 1125-1127.
- [34] S. R. Morrison, (1982) "Semiconductor Gas Sensors," *Sens. Actuators.*, **2** 329-341.
- [35] N. Serpone, (2006) "Is the Band Gap of Pristine TiO₂ Narrowed by Anion- and Cation-Doping of Titanium Dioxide in Second-Generation Photocatalysts?," *J. Phys. Chem B.*, **110** 24287-24293.
- [36] W. F. Zhang, M. S. Zhang, Z. Yin and Q. Chen, (2000) "Photoluminescence in anatase titanium dioxide nanocrystals," *Appl. Phys. B.*, **70** 261-265.
- [37] H. Yang, C. Huang, A. Tang, X. Zhang and W. Yang, (2005) "Microwave assisted synthesis of ceria nanoparticle," *Mater. Res. Bull.*, **40** 1690-1695.
- [38] H. Tang, K. Prasad, R. Sanjines, P. E. Schmid and F. Levy, (1994) "Electrical and Optical Properties of TiO₂ Anatase Thin Films," *J. Appl. Phys.*, **75** 2042-2047.
- [39] N. Barsan and U. Weimar, (2001) "Conduction model of metal oxide gas sensors," *J. Electroceram.*, **7** 143-167.

IOSR Journal of Applied Physics (IOSR-JAP) is UGC approved Journal with SI. No. 5010, Journal no. 49054.

S. Sharmila Juliet. "Effect of Calcination Temperature on Titanium Oxide Nanocrystallites in the Anatase Phase Synthesized By Sol-Gel Route." IOSR Journal of Applied Physics (IOSR-JAP), vol. 9, no. 4, 2017, pp. 32-39.